Self-Catalyzed, Self-Limiting Growth of Glucose Oxidase-Mimicking Gold Nanoparticles

Weijie Luo,† Changfeng Zhu,† Shao Su, Di Li,* Yao He, Qing Huang,* and Chunhai Fan*

Laboratory of Physical Biology, Shanghai Institute of Applied Physics, Chinese Academy of Sciences, Shanghai 201800, China. †These authors contributed equally to this work.

ARTICLE

ABSTRACT Size and shape of nanoparticles are generally controlled by external influence factors such as reaction temperature, time, precursor, and/or surfactant concentration. Lack of external influence may eventually lead to unregulated growth of nanoparticles and possibly loss of their nanoscale properties. Here we report a gold nanoparticle (AuNPs)-based self-catalyzed and self-limiting system that exploits the glucose oxidase-like catalytic activity of AuNPs. We find that the AuNP-catalyzed glucose oxidation *in situ* produces hydrogen peroxide (H_2O_2) that induces the AuNPs' seeded growth in the presence of chloroauric acid ($HAuCl_4$). This crystal growth of AuNPs is internally regulated *via* two negative feedback factors, size-dependent activity decrease of AuNPs and product (gluconic acid)-induced surface passivation, leading to a rapidly self-limiting system. Interestingly, the size, shape, and catalytic activities of AuNPs are simultaneously controlled in this system. We expect that it provides a new method for controlled synthesis of novel nanomaterials, design of "smart" self-limiting nanomedicine, as well as in-depth understanding of self-limiting systems in nature.

KEYWORDS: gold nanoparticles · glucose oxidase · self-limiting · catalytic activity · crystal growth

Self-limiting is a universal phenomenon in nature, such as found in cell growth, gene regulation, and epidemic spreading. Lack of self-limiting regulation may eventually lead to system crash. For example, overdose of many highly effective drugs (*e.g.*, insulin[1]) is known to induce severe side effects or even death, which motivates great efforts to design self-limiting "smart drugs", particularly *via* the approach of nanoscale materials-based nanomedicine.[2,3] Interestingly, self-limiting phenomena are also often observed in the nano world, for example, crystal growth of nanoparticles.[4−8] In these self-limiting growth systems, ultimate size and shape of nanoparticles are often determined by the surface atom lattice rearrangement that minimizes the overall Gibb's free energy and surface tension. Besides size and shape, chemical properties of nanomaterials that dictate their eventual applications are relatively difficult to self-control.

AuNPs play an important role in nanotechnology due to their attractive optical and electronic properties, excellent biocompatibility, and the availability of versatile bioconjugation means, which have led to a wide range of applications such as catalysis, fuel cells, and biodetection.[9−23] Particularly interesting, while gold was traditionally regarded to be chemically inert and resistant to oxidation, many studies have revealed that AuNPs supported on metal oxide substrates are highly active and can efficiently catalyze many reactions including low-temperature CO or NO oxidation.[24−31] More recently, small Au nanoclusters (3.6 nm) were found to be able to catalytically oxidize glucose and produce gluconates in a "green" approach,[32,33] similar to that of the natural enzyme of glucose oxidase (GOx), which also catalyzes the oxidation of glucose with the cosubstrate oxygen (O_2), producing gluconate and hydrogen peroxide (H_2O_2). On the basis of the intrinsic GOx-like catalytic activity of AuNPs, we have designed a self-limiting system by utilizing AuNPs as both seeds and catalyst and demonstrated that the size, shape, and catalytic activity of AuNPs are regulated by various factors including catalytic reaction conditions, seeded enlargement, and surface passivation of AuNPs.

RESULTS AND DISCUSSION

We first evaluated the GOx-mimicking activity of AuNPs in solution and studied the mechanism of this reaction occurring at the nanoscale surface. AuNPs prepared with the citrate reduction method were incubated with glucose at room temperature for 30 min. The resulting solution was interrogated with a gluconic acid-specific colorimetric assay.[34] When hydroxamine and Fe^{III} were added to the solution, we found that the color of the solution turned red, with a characteristic absorbance peak at 505 nm

*Address correspondence to fchh@sinap.ac.cn, lidi@sinap.ac.cn, huangqing@sinap.ac.cn.

Received for review September 29, 2010 and accepted November 18, 2010.

Published online November 30, 2010. 10.1021/nn102592h

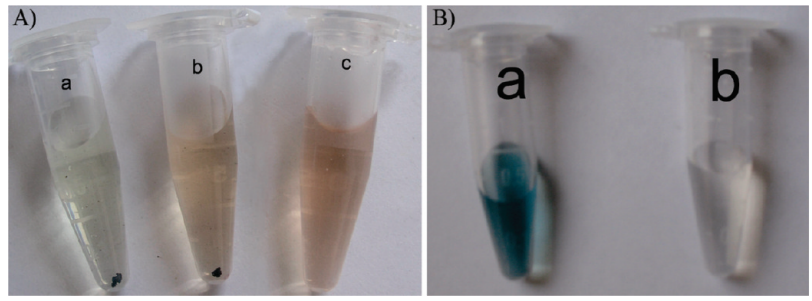

Figure 1. (A) AuNPs catalyze the oxidation of glucose to gluconic acid, producing a red colored product. (a) AuNPs in the absence of glucose, (b) AuNPs in the presence of glucose, and (c) GOx in the presence of glucose. (B,a) AuNPs catalyze the reduction of O_2 to H_2O_2, producing a green colored product upon incubation with HRP and $ABTS^{2-}$. (b) Supernatant solution after separating AuNPs could not produce the colored product in the same conditions. In panel A, the concentrations of AuNPs, glucose, and GOx are 120 nM, 300 mM, and 0.07 mg/mL, respectively; and in panel B, the concentrations of AuNPs, glucose, and HRP are 2.5 nM, 100 mM, and 0.5 mg/mL, respectively. In both experiments, AuNPs were centrifuged to prevent the influence of the color of AuNPs to the colorimetric reaction. The precipitates in panel A (a and b) were separated AuNPs.

(Figure 1A), which confirmed that gluconic acid was indeed produced in this AuNP-catalyzed reaction. The other possible product, H_2O_2, was interrogated *via* a horseradish peroxidase (HRP)-based colorimetric assay. We observed the appearance of a characteristic green color (maximum absorbance at 405 nm) when HRP and 2,2′-azinobis(3-ethylbenzothiazoline-6-sulfonic acid) (diammonium salt, $ABTS^{2-}$) were introduced (Figure 1B,a). Control studies with the AuNP-free supernatant solution indicated that neither citrate nor $HAuCl_4$ residues could introduce any color change (Figure 1B,b), suggesting that H_2O_2 was a product of the AuNP-based catalysis. The catalytic reaction is shown as the following equation:

$$\text{glucose} + O_2 \xrightarrow{\text{AuNPs}} \text{gluconic acid} + H_2O_2$$

The catalytic activity of AuNPs, as manifested by the HRP-induced colorimetric reaction, was dependent on the AuNP concentration, leading to a sigmoidal-shaped curve (Figure 2A). The reaction turnover increased dramatically as the concentration of AuNPs reached ~2 nM and reached a plateau at ~4 nM. This apparent catalytic activity could be completely blocked when the surface of AuNPs was passivated, for example, with thiolated DNA, leading to essentially no color change (Figure 2B). This suggested that the observed catalytic activity of AuNPs arose from Au atoms at the nanoscale surface. The catalysis of AuNPs followed a typical Michaelis−Menten behavior (Figure S1 of the Supporting Information), and the Michaelis−Menten constant (K_m) was calculated to be 6.97 mM, which was slightly higher than GOx (4.87 mM) (slightly lower affinity). The catalytic constant (K_{cat}) for AuNPs was ~2-fold larger than that of GOx, suggesting higher reaction rate (summarized in Table 1). The activation energy (E_a) of this reaction, as calculated from Arrhenius experiential formular, was ~16 kJ mol^{-1} (Figure S2). Of note, the GOx-mimicking activity was not observed in a range of interrogated nanomaterials, such as silver nanoparticles, TiO_2 nanoparticles, carbon nanotubes, and Fe_3O_4 nanoparticles (Figure S3).

The catalytic activity of AuNPs was further systematically investigated at different reaction time, temperature, solution pH, and with different sizes. We found that the catalysis reached a plateau at ~30 min at room temperature (Figure 3A). Interestingly, AuNPs exhib-

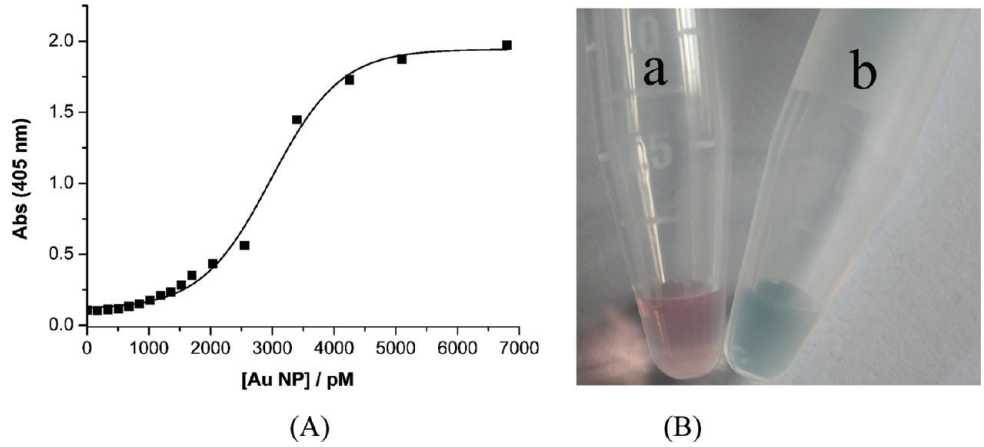

Figure 2. (A) Concentration-dependent catalytic activities of AuNPs. (B) Comparison of the catalytic activity of DNA-modified AuNPs (a) and "naked" AuNPs (b). In panel A, the concentration of HRP is 0.5 mg/mL, and in panel B, the concentrations of AuNPs, glucose, and HRP are 2.5 nM, 60 mM, and 0.5 mg/mL, respectively.

TABLE 1. Comparison of Kinetic Parameters of AuNP and GOx[a]

	[E] (M)	substrate	K_m (mM)	V_{max} (μM s^{-1})	K_{cat} (s^{-1})
AuNP (13 nm)	3.4×10^{-8}	glucose	6.97	0.63	18.52
GOx	7.1×10^{-8}	glucose	4.87	0.69	9.71

[a] [E] is the Au or GOx concentration; K_m is the Michaelis constant; V_{max} is the maximal reaction velocity; and K_{cat} is the catalytic constant, where $K_{cat} = V_{max}/[E]$.

ited superior pH, thermal, and storage stability to natural enzyme GOx. AuNPs showed high catalytic activity in a fairly broad range (pH 2−9, as manifested by the amount of catalytic product, gluconic acid), while GOx was only active at acidic pH (Figure 3B). Similarly, the activity of AuNPs revealed a lateral increase along with the temperature elevation, in sharp contrast to the bell-shaped curve for GOx (Figure 3C). In addition, the activity of this inorganic AuNP remained unchanged during 24 h storage at 25 °C (Figure 3D). In contrast, GOx was only stable at 4 °C and lost ~90% of its activity at 25 °C. The catalytic activity of AuNPs was also shown to be size-dependent. By using AuNPs of different size (13, 20, 30, and 50 nm) at the same concentration (concentration was normalized to the amount of Au atoms), we found that the catalytic activity of AuNP decreased along with their sizes (Figure 3E), which further suggested that Au atoms at the surface were responsible for the observed catalysis.

Given that H_2O_2 was produced during AuNP-based glucose oxidation, we attempted to couple this reaction with a AuNP-seeded Au crystal growth process (Figure 4). We designed a system containing AuNPs that served as both seeds and catalyst, glucose and O_2 as the enzymatic substrates, and $HAuCl_4$ as the fuel. H_2O_2 was previously found to reduce $HAuCl_4$ in the presence of AuNPs.[35,36] We thus expected that AuNPs first catalyzed the glucose oxidation reaction, and the *in situ* generated product H_2O_2 reduced the $HAuCl_4$ fuel to Au^0, which deposited on the AuNP seed as a nanoislands, leading to gradually enlarged AuNPs.

This system was monitored in real-time by UV−vis spectroscopy, as shown in the time evolution curves (Figure 5A). Initially, we observed gradual increase in the absorbance intensity during the first 30 min, concomitant with slight red shift of the surface plasmon (SP) absorbance peak of AuNPs, suggesting the slow growth of AuNPs. During this process, the solution color underwent a gradual visible change from red to blue (Figure 5A inset, and time evolution in Figure S4). Interestingly, intensity of this SP absorbance peak increased dramatically at a critical turning point of 30 min and then remained almost unchanged after that (Figure 5B). The initial gradual change coincides well with our proposed coupled reactions of AuNP-based catalysis and seeded growth. This abrupt change at 30 min corresponds to our observation that the reaction rate reaches a plateau at 30 min (Figure 3A), which produces a sufficiently high concentration of H_2O_2 to stimulate the enlargement of AuNPs. However, it is interest-

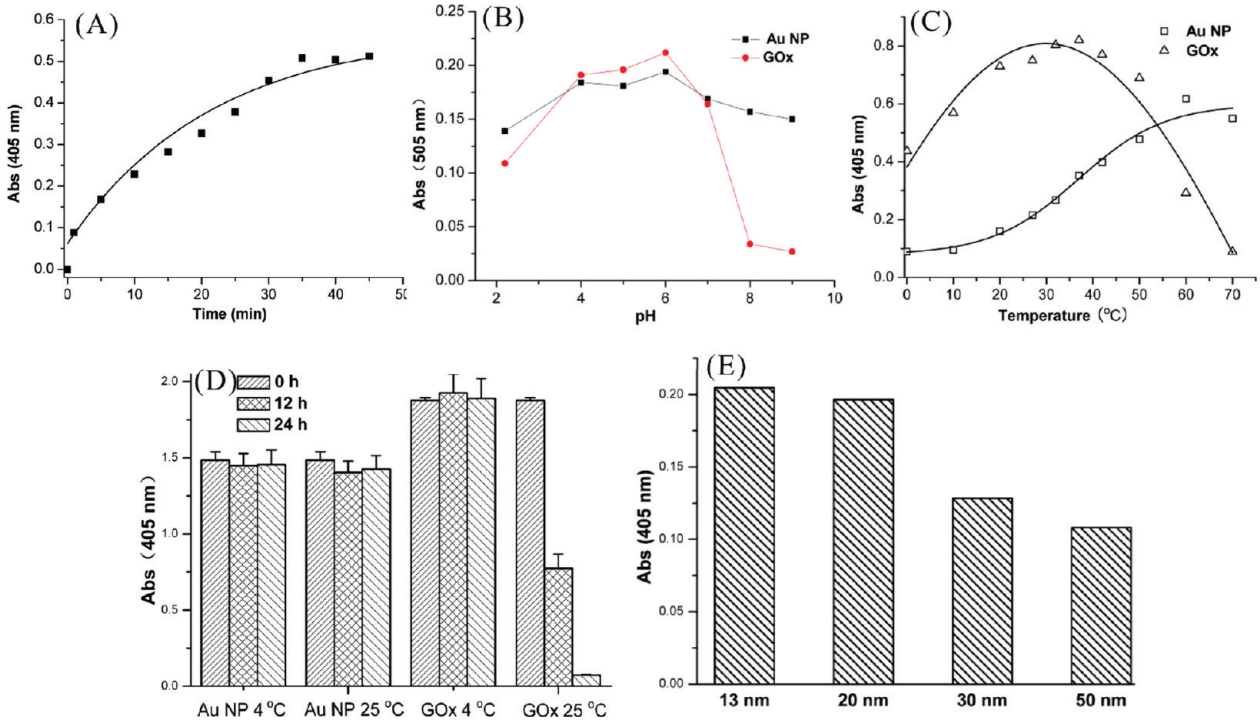

Figure 3. (A) Catalytic activity of AuNPs as a function of incubation time. (B) The pH-dependent catalytic activities of AuNPs (black square) and GOx (red sphere). (C) Catalytic activities of AuNPs (square) and GOx (triangle) as a function of incubation temperature. (D) Comparison of the catalytic activities of GOx and AuNPs after long-term storage. (E) Size-dependent catalytic activity of AuNPs. The catalytic activity in panel B was reported by gluconic acid (titrated by NaOH) in order to avoid the influence of pH on the HRP-based colorimetric reaction.

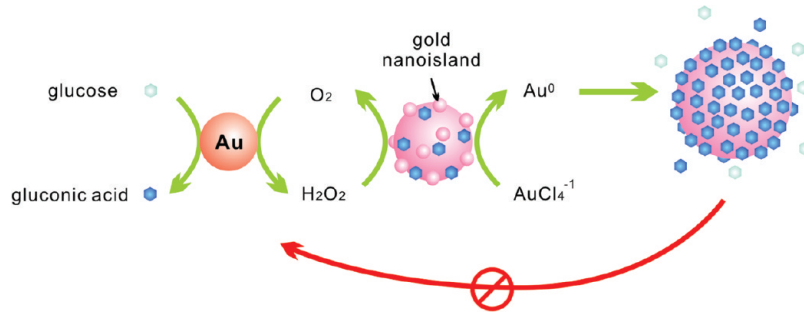

Figure 4. Schematic demonstration of the AuNP-based self-limiting growth system. The size, shape, and catalytic activity of AuNPs are self-limited by the integrated influence from the catalytic reaction, seeded enlargement, and surface passivation of AuNPs.

ing that the nanoparticle growth rapidly self-limits at this point, with essentially no apparent growth any further. The generation of H_2O_2 is of vital importance for the growth of AuNPs. In a control experiment carried out in the anaerobic condition (no O_2) that prevent the H_2O_2 formation, the SP absorbance of AuNPs remained almost unchanged in the presence of glucose and $HAuCl_4$ (Figure 5C). The enlarged AuNPs were characterized with transmission electron microscopy (TEM, Figure 5D), which showed that the spherical AuNPs (a) with average diameter of 13 ± 2 nm, were enlarged to rough, flower-like nanostructures,[37] with a relatively broad size dimension of 30−40 nm (b) (the size distribution histograms of spherical AuNPs and the enlarged nanoflowers are shown in Figure S5). We first performed TEM studies to exclude the possibility that the size of AuNPs was changed during the catalytic reaction (Figure S6). We also performed another control experiment to exclude the possibility that the consumption of $HAuCl_4$ limits the enlargement process. After 30 min of incubation, we carefully removed the enlarged AuNPs by repetitive centrifuge. ICP-MS analysis indicated that there was still 6 ng/mL Au element remaining in the supernatant solution. This provides strong evidence that the cease of enlargement process was not due to the lack of $HAuCl_4$. Since a typical AuNP-seeded reaction with H_2O_2 and $HAuCl_4$ led to relatively smooth enlarged AuNPs, we suggest that the preferential adsorption of gluconic acid on a certain crystal facet of the AuNPs is possibly responsible for the resulting flower-like morphology.[32] To prove this assumption, we added another reducing agent, ascorbic acid, to the solution with enlarged Au nanoflowers to further reduce residue $HAuCl_4$. TEM studies (Figure S7) demonstrate that, after this chemical reduction, the diameter of the Au nanoflowers remained nearly unchanged.

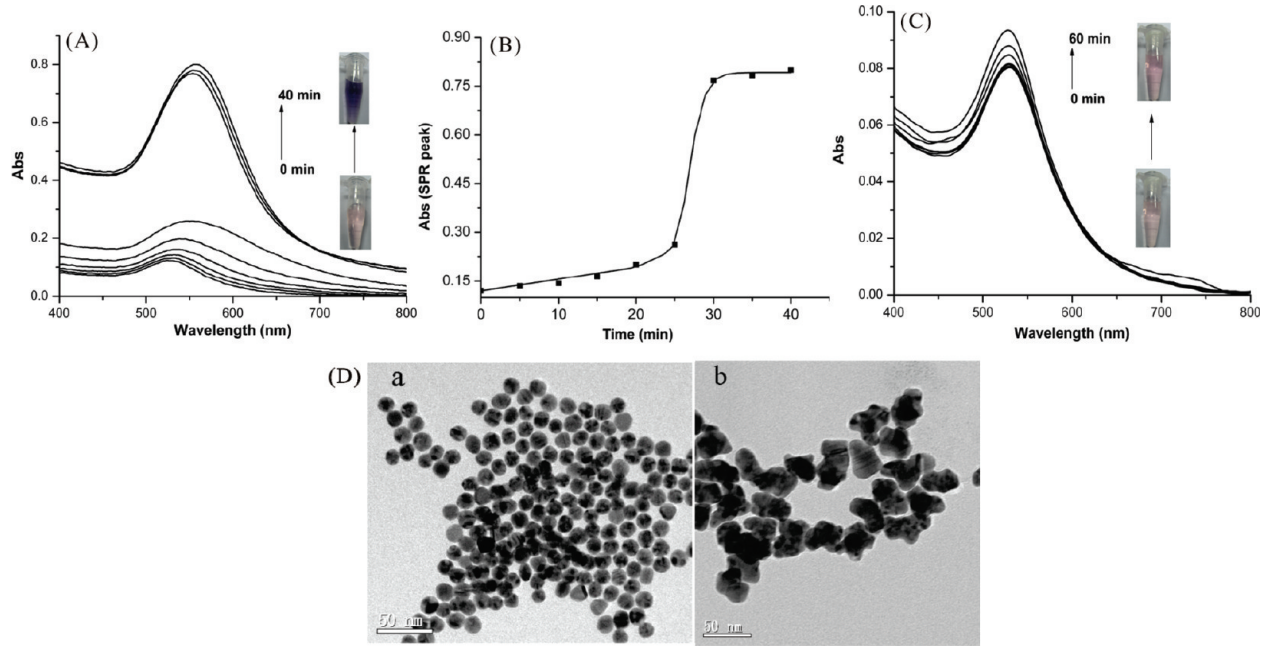

Figure 5. (A) Time-dependent UV−vis spectra of AuNPs in an air-saturated growth solution. Time interval: 5 min. The growth solution is a phosphate buffer (10 mM, pH 7.2) containing 0.35 nM of 13 nm AuNPs, 50 mM of glucose, and 0.2 mM of $HAuCl_4$. (B) Time-dependent absorbance changes (recorded at the surface plasmon peak at different time intervals) of the self-limiting growth. (C) Time-dependent UV−vis spectra of AuNPs in a N_2-saturated growth solution. Time interval: 10 min. All other conditions remained the same as panel A. Insets in panels A and C show the visible color change of AuNPs during the growth. (D) TEM images of the as-prepared 13 nm AuNPs (a) and the enlarged AuNPs (b). Scale bar: 50 nm.

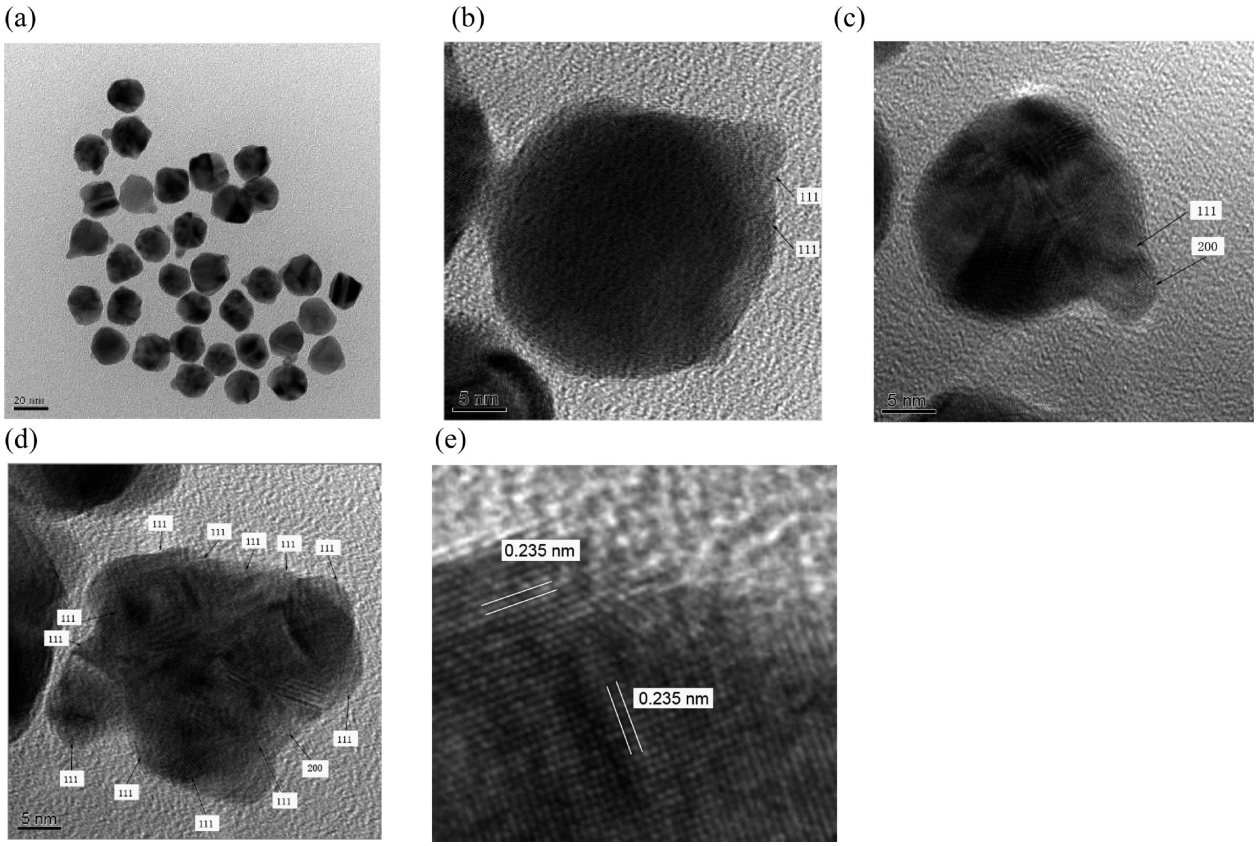

Figure 6. TEM image (a) and HRTEM images (b,c) of AuNPs after 15 min of enlargement. HRTEM (d,e) images of AuNPs after 30 min of enlargement. The interplanar spacing was 0.235 nm in panel e, suggesting the lattice fringe of Au (111) crystal face. Scale bar is 20 nm for panel a and 5 nm for panels b, c, and d.

However, it is interesting to note that petals of the nanoflowers grew dramatically, suggesting that only the petal part of the nanoflowers was active while the other part of the nanoflower was inactivated by surface adsorption of gluconic acid.

We have also analyzed the topography changes of AuNPs during the enlargement process by TEM. As shown in Figure 6a, after 15 min of enlargement, one or two petals were deposited on spherical AuNPs. High resolution TEM (HR-TEM) images suggested that most of these petals were deposited at the sharp intersection of (111)/(111) (Figure 6b), as determined from the lattice fringe, with a few exceptions at (200)/(111) faces (Figure 6c). The HR-TEM image of the AuNPs with 30 min enlargement (Figure 6d) also indicated that most petals of the Au nanoflowers were of (111) face with a few exceptions of (200). Interestingly, the (111) face with the lowest energy was exposed on the protuberant part of AuNPs (Figure 6e), suggesting that the self-limiting process may smooth out the sharp edges of the NPs to minimize the surface energy.

We reason that there exist two factors to act as negative feedback for this rapidly self-limiting system. First, the increased size of the AuNP slows the catalytic reaction due to the reduced amount of surface Au atoms as compared to the volume. Second, the catalytic product, gluconic acid, is deposited on the surface of AuNPs, which blocks reaction-active surface Au atoms and inhibits further catalysis (Figure 4).

We first examined the catalytic activity of enlarged AuNPs that were separated from the system with centrifugation, which exhibited minimal activity toward glucose oxidation (Figure 7A). While we did find that the activity of AuNPs decreases with the size increment, as-prepared AuNPs of 50 nm, a size dimension similar to the enlarged AuNPs, still possess medium activity toward glucose oxidation (Figure 3E). Therefore, the size increase alone cannot account for the complete inactivation of AuNPs after the critical point.

We then further employed X-ray photoelectron spectroscopy (XPS) to explore the reaction mechanism at this nanoscale surface. Figure 7B shows the XPS of AuNPs before (red curve) and after (blue curve) the catalytic reaction. The binding energy (BE) of $Au4f_{7/2}$ at 84.0 eV corresponding to metallic Au remained unchanged, implying that the valence state of AuNPs did not change during catalysis. In contrast, the atomic ratio of C/Au was substantially increased from 1.60 to 12.10 after the catalytic reaction, which suggested the adsorption of an organic layer on the surface of AuNPs. Further, we analyzed the C1s peaks with linear background subtraction and peak separation by using mixed Gaussian−Lorentzian functions (see peak assignment and content of C1s in Table 2). Indeed, the con-

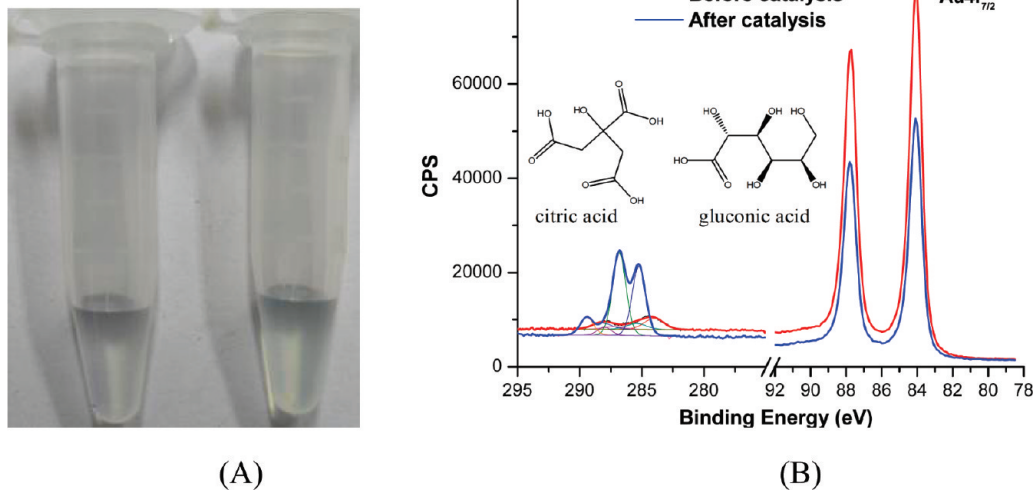

Figure 7. (A) Decreased catalytic activities of the enlarged AuNPs. The left tube corresponds to the control sample, that is, in the absence of glucose; the right tube corresponds to the catalytic activity of the as-enlarged AuNPs toward 60 mM of glucose. (B) XPS spectra of the AuNPs before (red) and after (blue) the catalytic reaction. Inset is the chemical structure of citric acid and gluconic acid.

tent of carboxylic carbon (COOH, marked in red) dramatically decreased by 2-fold, while that of alkyl carbon (C−O, marked in blue) increased by 2-fold. Of note, the as-prepared AuNPs are stabilized with a layer of citric acid that contains three COOH groups while only one C−O bond. The replacement of citric acid with gluconic acid would increase the C−O content and decrease the COOH content since the latter contains one COOH group and five C−O bonds, which coincides well with the experimental observations. Therefore, the XPS data confirmed the presence of a gluconic acid capping layer on the surface of AuNPs after the catalytic reaction. We also found that, even for the as-prepared 13 nm spherical AuNPs, its catalytic activity diminished after three successive cycles (Figure S8). Thus, the appearance of the catalytic product, gluconic acid, which is the second negative feedback, clearly contributes to the inactivation of AuNPs. However, it is still unclear why citric acid does not inhibit the catalytic activity of AuNPs. A possible explanation might arise from the different binding energies of these two organic molecules to Au.

TABLE 2. Assignment of the C1s Peaks of AuNP before and after the Catalytic Reaction

	binding energy (eV)	peak assignment	% concn
AuNP before catalysis	284.63	C−C	43.02
	288.83	O−C=O	24.12
	286.03	C−O	22.85
	287.83	C=O	10.01
AuNP after catalysis	285.24	C−C	39.01
	289.43	O−C=O	10.04
	286.82	C−O	46.34
	288.02	C=O	4.61

CONCLUSION

Here we provide a novel system that exhibits self-limiting growth of nanoparticles based on the GOx-mimicking catalytic activity of AuNPs. In this system, the AuNP-catalyzed glucose oxidation produces H_2O_2 that induces the AuNP-seeded growth in the presence of $HAuCl_4$. This crystal growth is internally regulated *via* two negative feedback factors, size-dependent activity decrease of AuNPs and product (gluconic acid)-induced surface passivation. We have demonstrated that size, shape, and catalytic activity of AuNPs are simultaneously controlled in this self-limiting system, which provides a new method for controlled synthesis of novel nanomaterials, design of "smart" self-limiting nanomedicine, as well as in-depth understanding of self-limiting systems in nature.

METHODS

Materials. Glucose oxidase (GOx, from *Aspergillus niger*, E.C. 1.1.3.4), horseradish peroxidase (HRP, EC 1.11.1.7), glucose, $HAuCl_4$, $FeCl_3 \cdot 6H_2O$, and 2,2′-azinobis(3-ethylbenzothiazoline-6-sulfonate acid) (diammonium salt, $ABTS^{2-}$) were purchased from Sigma-Aldrich and used as received. Thiolated DNA (5′HS-CGCATTCAGGAT-3) was obtained by Takara Biotechnology Co. (Dalian, China) and purified with HPLC.

Synthesis of AuNPs. AuNPs of different sizes were synthesized according to the citrate reduction method.[38] Modification of 13 nm AuNPs with thiolated DNA followed the previously reported protocol.[39] Briefly, the aqueous Au nanoparticle solution and thiolated DNA (final concentration of 1.5 μM, about 1 o.d.) were incubated together for 16 h under constant stirring. The solution was slowly brought up to final salt concentrations of 0.1 M NaCl and 10 mM phosphate (pH 7) and allowed to stand for 40 h.

Glucose Oxidation Reaction and Kinetic Studies. The kinetics of the catalytic reaction was obtained from a Michaelis−Menten curve. The rate of the catalytic reaction was defined as the amount of generated product, gluconic acid, in a fixed time interval of 30

min. The amount of gluconic acid was determined by continuous titration with NaOH. In detail, 34 nM of AuNPs or 71 nM of GOx was incubated with a series of concentrations of glucose (in water) for 30 min. Then the obtained gluconic acid was continuously titrated with 0. 1 M of NaOH and indicated with phenolphthalein at pH 8.2. Assay for H_2O_2 was tested with a colorimetric reaction involving HRP and $ABTS^{2-}$. In brief, AuNPs were first incubated with glucose for 30 min, and then HRP and $ABTS^{2-}$ were added to the solution to final concentrations of 0.5 μg/mL and 0.4 mM, respectively. The resulting mixture was further incubated for 5 min at room temperature before measurement of absorbance at 405 nm for the colored product $ABTS^{2-}$.

Similarly, the other reaction product, gluconic acid, was assayed by reaction with hydroxylamine and subsequent complex with Fe^{III}, which led to a red complex hydroxamate-Fe^{3+} (with a maximum absorbance at 505 nm). In brief, 250 μL of solution 1 (5 mM EDTA and 0.15 mM Et_3N in water) and 25 μL of solution 2 (3 M NH_2OH in water) were added to the catalytic reaction solution, and the mixture was allowed to react for 15 min. Finally, 125 mL of solution 3 (1 M HCl, 0.1 M $FeCl_3$, and 0.25 M CCl_3COOH in water) was added to the reaction medium, and the reaction was allowed to proceed for 5 min.

Self-Limiting Growth of AuNPs. The AuNP enlargement experiment was carried out in 10 mM phosphate buffer (pH 7.2) containing 2 nM of 13 nm AuNP, 50 mM of glucose, and 0.2 mM of $HAuCl_4$. The UV−vis spectra of this growth solution were continuously recorded within 40 min with a time interval of 5 min. In a control, anaerobic experiment, O_2 was removed from the solution *via* degassing with N_2, and the UV−vis spectra were monitored under N_2 atmosphere.

Characterization. TEM measurements were performed on a Philips CM300 FEG (FEI, USA) electron microscope operating at 300 kV. XPS measurement was carried out with a Axis Ultra DLD spectrometer (Kratos, UK) employing a standard Mg Kα (1256.6 eV). X-ray source operated at 150 W. UV−vis absorption spectroscopy was performed with a Hitachi U-3010 spectrophotometer, and photographs were taken with a Canon Powershot A620 digital camera. The colorimetric assay in 96-well plates was monitored at 405 nm (for H_2O_2) or 505 nm (for gluconic acid) with a Tecan microplate reader. The trace amount of $HAuCl_4$ after the self-limiting growth was analyzed by inductively coupled plasma mass spectrometry (ICP-MS, X-7, Thermo Elemental, USA).

Acknowledgment. This work was supported by the National Natural Science Foundation of China (20873175, 21075128, and 20725516), the Shanghai Municipal Commission for Science and Technology (0952 nm0460, 10QA1408200), the Ministry of Health (2009ZX10004-301), and the Ministry of Science and Technology (2007CB936000).

Supporting Information Available: Additional figures (S1−S8). This material is available free of charge *via* the Internet at http://pubs.acs.org.

REFERENCES AND NOTES

1. Johnson, J. D.; Bernal-Mizrachi, E.; Alejandro, E. U.; Han, Z.; Kalynyak, T. B.; Li, H.; Beith, J. L.; Gross, J.; Warnock, G. L.; Townsend, R. R.; *et al.* Insulin Protects Islets from Apoptosis *via* Pdx1 and Specific Changes in the Human Islet Proteome. *Proc. Natl. Acad. Sci. U.S.A.* **2006**, *103*, 19575–19580.
2. Davis, M. E.; Chen, Z.; Shin, D. M. Nanoparticle Therapeutics: An Emerging Treatment Modality for Cancer. *Nat. Rev. Drug Discovery* **2008**, *7*, 771–782.
3. Cancer Nanotechnology: Small, but Heading for the Big Time. *Nat. Rev. Drug Discovery* **2007**, *6*, 174−175.
4. Madey, T. E.; Pelhos, K.; Wu, Q. F.; Barnes, R.; Ermanoski, I.; Chen, W. H.; Kolodziej, J. J.; Rowe, J. E. Nanoscale Surface Chemistry. *Proc. Natl. Acad. Sci. U.S.A.* **2002**, *99*, 6503–6508.
5. Gwo, S.; Chou, C. P.; Wu, C. L.; Ye, Y. J.; Tsai, S. J.; Lin, W. C.; Lin, M. T. Self-Limiting Size Distribution of Supported Cobalt Nanoclusters at Room Temperature. *Phys. Rev. Lett.* **2003**, *90*, 185506.
6. Jesson, D. E.; Chen, G.; Chen, K. M.; Pennycook, S. J. Self-Limiting Growth of Strained Faceted Islands. *Phys. Rev. Lett.* **1998**, *80*, 5156–5159.
7. Kastner, M.; Voigtlander, B. Kinetically Self-Limiting Growth of Ge Islands on Si(001). *Phys. Rev. Lett.* **1999**, *82*, 2745–2748.
8. Takakusagi, S.; Fukui, K.; Tero, R.; Nariyuki, F.; Iwasawa, Y. Self-Limiting Growth of Pt Nanoparticles from $MeCpPtMe_3$ Adsorbed on TiO_2(110) Studied by Scanning Tunneling Microscopy. *Phys. Rev. Lett.* **2003**, *91*, 06612.
9. Daniel, M. C.; Astruc, D. Gold Nanoparticles: Assembly, Supramolecular Chemistry, Quantum-Size-Related Properties, and Applications toward Biology, Catalysis, and Nanotechnology. *Chem. Rev.* **2004**, *104*, 293–346.
10. Edwards, P. P.; Thomas, J. M. Gold in a Metallic Divided State—From Faraday to Present-Day Nanoscience. *Angew. Chem., Int. Ed.* **2007**, *46*, 5480–5486.
11. Giljohann, D. A.; Mirkin, C. A. Drivers of Biodiagnostic Development. *Nature* **2009**, *462*, 461–464.
12. Rosi, N. L.; Mirkin, C. A. Nanostructures in Biodiagnostics. *Chem. Rev.* **2005**, *105*, 1547–1562.
13. Zhao, W.; Brook, M. A.; Li, Y. F. Design of Gold Nanoparticle-Based Colorimetric Biosensing Assays. *ChemBioChem* **2008**, *9*, 2363–2371.
14. Xiao, Y.; Patolsky, F.; Katz, E.; Hainfeld, J. F.; Willner, I. "Plugging Into Enzymes": Nanowiring of Redox Enzymes by a Gold Nanoparticle. *Science* **2003**, *299*, 1877–1881.
15. Zhang, J.; Sasaki, K.; Sutter, E.; Adzic, R. R. Stabilization of Platinum Oxygen-Reduction Electrocatalysts Using Gold Clusters. *Science* **2007**, *315*, 220–222.
16. Sharma, J.; Chhabra, R.; Cheng, A.; Brownell, J.; Liu, Y.; Yan, H. Control of Self-Assembly of DNA Tubules through Integration of Gold Nanoparticles. *Science* **2009**, *323*, 112–116.
17. Zhang, J.; Song, S.; Wang, L.; Pan, D.; Fan, C. A Gold Nanoparticle-Based Chronocoulometric DNA Sensor for Amplified Detection of DNA. *Nat. Protoc.* **2007**, *2*, 2888–2895.
18. Zhang, J.; Song, S.; Zhang, L.; Wang, L.; Wu, H.; Pan, D.; Fan, C. Sequence-Specific Detection of Femtomolar DNA *via* a Chronocouloumetric DNA Sensor (CDS): Effects of Nanoparticle-Mediated Amplification and Nanoscale Control of DNA Assembly at Electrodes. *J. Am. Chem. Soc.* **2006**, *128*, 8575–8580.
19. Li, H.; Huang, J.; Lv, J.; An, H.; Zhang, X.; Zhang, Z.; Fan, C.; Hu, J. Nanoparticle PCR: Nanogold-Assisted PCR with Enhanced Specificity. *Angew. Chem., Int. Ed.* **2005**, *44*, 5100–5103.
20. Song, S.; Liang, Z.; Zhang, J.; Wang, L.; Li, G.; Fan, C. Gold-Nanoparticle-Based Multicolor Nanobeacons for Sequence-Specific DNA Analysis. *Angew. Chem., Int. Ed.* **2009**, *48*, 8670–8674.
21. Li, D.; Song, S.; Fan, C. Target-Responsive Structures for Nucleic Acid Sensors. *Acc. Chem. Res.* **2010**, *43*, 631–641.
22. Song, S.; Qin, Y.; He, Y.; Huang, Q.; Fan, C.; Chen, H. Functional Nanoprobes for Ultrasensitive Detection of Biomolecules. *Chem. Soc. Rev.* **2010**, *39*, 4234–4243.
23. Chen, T.; Yang, M.; Wang, X.; Tan, L. H.; Chen, H. Controlled Assembly of Eccentrically Encapsulated Gold Nanoparticles. *J. Am. Chem. Soc.* **2008**, *130*, 11858–11859.
24. Chen, M. S.; Goodman, D. W. Catalytically Active Gold: From Nanoparticles to Ultrathin Films. *Acc. Chem. Res.* **2006**, *39*, 739–746.
25. Gong, J. L.; Mullins, C. B. Surface Science Investigations of Oxidative Chemistry on Gold. *Acc. Chem. Res.* **2009**, *42*, 1063–1073.
26. Valden, M.; Lai, X.; Goodman, D. W. Onset of Catalytic Activity of Gold Clusters on Titania with the Appearance of Nonmetallic Properties. *Science* **1998**, *281*, 1647–1650.
27. Corma, A.; Garcia, H. Supported Gold Nanoparticles as Catalysts for Organic Reactions. *Chem. Soc. Rev.* **2008**, *37*, 2096–2126.
28. Lee, Y. M.; Garcia, M. A.; Huls, N. A. F.; Sun, S. H. Synthetic Tuning of the Catalytic Properties of Au-Fe_3O_4 Nanoparticles. *Angew. Chem., Int. Ed.* **2010**, *49*, 1271–1274.

29. Chen, M. S.; Goodman, D. W. Structure−Activity Relationships in Supported Au Catalysts. *Catal. Today* **2006**, *111*, 22–33.
30. Hammer, B. Special Sites at Noble and Late Transition Metal Catalysts. *Top. Catal.* **2006**, *37*, 3–16.
31. Haruta, M. Catalysis of Gold Nanoparticles Deposited on Metal Oxides. *Cattech* **2002**, *6*, 102–115.
32. Comotti, M.; Della Pina, C.; Matarrese, R.; Rossi, M. The Catalytic Activity of "Naked" Gold Particles. *Angew. Chem., Int. Ed.* **2004**, *43*, 5812–5815.
33. Beltrame, P.; Comotti, M.; Della Pina, C.; Rossi, M. Aerobic Oxidation of Glucose II. Catalysis by Colloidal Gold. *Appl. Catal.* **2006**, *297*, 1–7.
34. Rakitzis, E. T.; Papandreou, P. Reactivity of 6-Phosphogluconolactone with Hydroxylamine: The Possible Involvement of Glucose-6-phosphate Dehydrogenase in Endogenous Glycation Reactions. *Chem. Biol. Interact.* **1998**, *113*, 205–216.
35. Basnar, B.; Weizmann, Y.; Cheglakov, Z.; Willner, I. Synthesis of Nanowires Using Dip-Pen Nanolithography and Biocatalytic Inks. *Adv. Mater.* **2006**, *18*, 713–718.
36. Zayats, M.; Baron, R.; Popov, I.; Willner, I. Biocatalytic Growth of Au Nanoparticles: From Mechanistic Aspects to Biosensors Design. *Nano Lett.* **2005**, *5*, 21–25.
37. Wang, Z. D.; Zhang, J. Q.; Ekman, J. M.; Kenis, P. J. A.; Lu, Y. DNA-Mediated Control of Metal Nanoparticle Shape: One-Pot Synthesis and Cellular Uptake of Highly Stable and Functional Gold Nanoflowers. *Nano Lett.* , *10*, 1886–1891.
38. Grabar, K. C.; Freeman, R. G.; Hommer, M. B.; Natan, M. J. Preparation and Characterization of Au Colloid Monolayers. *Anal. Chem.* **1995**, *67*, 735–743.
39. Elghanian, R.; Storhoff, J. J.; Mucic, R. C.; Letsinger, R. L.; Mirkin, C. A. Selective Colorimetric Detection of Polynucleotides Based on the Distance-Dependent Optical Properties of Gold Nanoparticles. *Science* **1997**, *277*, 1078–1081.